17^{th} Annual Workshop on
Mathematical Problems in Industry
Rensselaer Polytechnic Institute, June 4-8, 2001

Shape optimization of pressurized air bearings

Problem presented by
Ferdinand Hendriks
IBM Research Division
T. J. Watson Research Center
Hawthorne, NY

	P. Howell	M. Kedzior	P. Kramer
Participants:	C. Please	L. Rossi	W. Saintval
	D. Salazar	T. Witelski	

Summary Presentation given by L. Rossi (6/8/01)
Summary Report prepared by T. Witelski (1/20/02 version)

1 Introduction

Use of externally pressurized air bearings allows for the design of mechanical systems requiring extreme precision in positioning. One application is the fine control for the positioning of mirrors in large-scale optical telescopes. Other examples come from applications in robotics and computer hard-drive manufacturing. Pressurized bearings maintain a finite separation between mechanical components by virtue of the presence of a pressurized flow of air through the gap between the components. An everyday example is an air hockey table, where a puck is levitated above the table by an array of vertical jets of air. Using pressurized bearings there is no contact between "moving parts" and hence there is no friction and no wear of sensitive components.

This workshop project is focused on the problem of designing optimal static air bearings [15] subject to given engineering constraints. Recent numerical computations of this problem, done at IBM by Robert and Hendriks [11, 12], suggest that near-optimal designs can have unexpected complicated and intricate structures. We will use analytical approaches to shed some light on this situation and to offer some guides for the design process.

In Section 2 the design problem is stated and formulated as an optimization problem for an elliptic boundary value problem. In Section 3 the general problem is specialized to bearings with rectangular bases. Section 4 addresses the solutions of this problem that can be obtained using variational formulations of the problem. Analysis showing the sensitive dependence to perturbations (in numerical computations or manufacturing constraints) of near-optimal designs is given in Section 5. In Section 6, a restricted class of "groove network" designs motivated by the original results of Robert and Hendriks is examined. Finally, in Section 7, we consider the design problem for circular axisymmetric air bearings.

2 Problem formulation

The goal is to design a pressurized air bearing that generates the maximum lift for a given gap volume. Given constraints of a fixed domain $\Omega(X, Y)$ for the bearing, and fixed positions for the pressure inlets and outlets, the design of the bearing involves selecting a bearing surface $Z_U =$

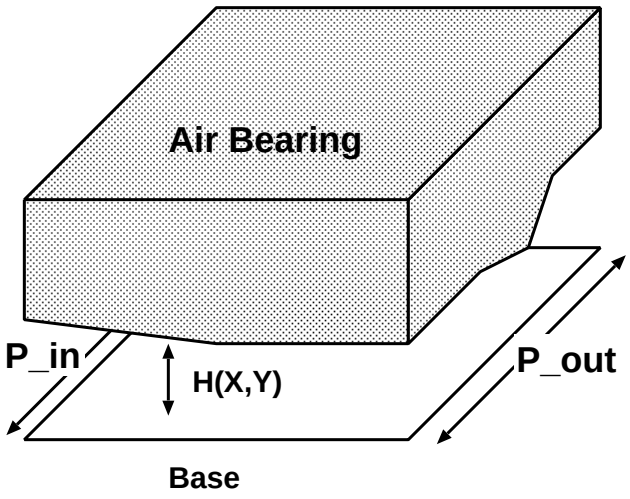

Figure 1: The geometry of the air bearing problem. The design of the lower surface of the bearing block defines the gap height $H(X,Y)$ that separates the block from a flat base plate. Fixed pressure boundary conditions define the positions of air-flow inlets and outlets.

$S(X,Y)$ that is separated from a flat base $Z_L = 0$ by a given minimum gap-height. Equivalently, we can express the problem in terms of the gap height, $H(X,Y) = Z_U - Z_L$, see Figure 1.

The lift is given by the integral of the excess pressure over the domain of the bearing,

$$\mathcal{L} = \int\int_{\Omega} P(X,Y) - P_{\text{atm}}\, dY\, dX, \tag{2.1}$$

where $P(X,Y)$ is the pressure in the narrow gap under the bearing. The pressure is governed by the time-independent Reynolds' equation

$$\nabla \cdot (\rho H^3 \nabla P) = 0, \tag{2.2}$$

where ρ is the density of the fluid in the gap. For bearings, problems of interest will be isothermal [14], so we will consider the cases of (i) incompressible flows $\rho = \rho_0$ (constant), or (ii) isothermal ideal gases, $\rho = kP$. Both compressible and incompressible cases are given by elliptic problems of the same form,

$$\nabla \cdot (H^3 \nabla \Phi) = 0, \tag{2.3}$$

where $\Phi = P^{1+\alpha}$ with $\alpha = 0$ for the incompressible case and $\alpha = 1$ for the compressible problem. Boundary conditions for $P(X,Y)$ in equation (2.2) must be specified on the entire perimeter of Ω. For a pressurized bearing, these conditions are specified for the inlet (the pressure source), the outlet (the pressure sink), and the remaining insulated, no-flux boundaries,

$$P(\partial\Omega_{\text{in}}) = P_{\text{in}}, \qquad P(\partial\Omega_{\text{out}}) = P_{\text{out}}, \qquad \mathbf{n} \cdot \nabla P(\Omega_{\text{rest}}) = 0. \tag{2.4}$$

This elliptic boundary value problem for $P(X,Y)$, called the forward problem, has a unique solution if a positive gap height $H(X,Y)$ is given. In our case, H is the desired unknown, and (2.2) is considered an inverse problem. Drawing analogies to problems in electrostatics, P can be viewed as a potential function, H^3 as a conductivity, and (2.2) can be considered as an "inverse conductivity problem" [5] studied extensively in connection with tomography, medical imaging, and geophysics. Our problem however, has different constraints than standard inverse conductivity problems. In

the framework of optimization problems for solutions of elliptic equations, this design problem can be related to questions in materials science for the design of composite materials (called functional graded materials) that optimize certain physical properties of the material [1, 3, 6].

In addition to maximizing the lift (2.1), we also specify the total volume of the gap, or equivalently, the average gap height, $\bar{H}$,

$$\mathcal{V} = \int\int_{\Omega} H \, dY \, dX = \bar{H} \int\int_{\Omega} dY \, dX. \tag{2.5}$$

From other design considerations, specified upper and lower bounds on the gap height will also be given,

$$0 < H_{\min} \leq H(X, Y) \leq H_{\max}. \tag{2.6}$$

We will describe the search for bearing designs that maximize the lift (2.1) subject to the constraints (2.2, 2.4–2.6) for two simple geometries; a square and a disk. We focus on the incompressible case to simplify the problem.

3 Two-dimensional air bearings

Here we consider problems on the square domain, $\Omega = \{(X, Y) | \, 0 \leq X \leq L_X, 0 \leq Y \leq L_Y\}$ with $L_X = L_Y$, with the pressure inlet being the edge $Y = 0$, the outlet is $Y = L_Y$, and the other two edges are insulated.

We begin by nondimensionalizing the problem,

$$x = X/L_X \qquad y = Y/L_Y \tag{3.1}$$

$$P = P_{\text{in}} + (P_{\text{out}} - P_{\text{in}}) \, p \tag{3.2}$$

$$H = H_{\max} \, h, \qquad \epsilon \equiv \frac{H_{\min}}{H_{\max}} \tag{3.3}$$

The incompressible Reynolds equation takes the form

$$\nabla \cdot (h^3 \nabla p) = 0, \tag{3.4a}$$

with fixed pressure at the inlet and outlet boundaries

$$p(x, 0) = 1, \qquad p(x, 1) = 0, \tag{3.4b}$$

and no flux through the lateral sides of the domain

$$\partial_x p(0, y) = 0, \qquad \partial_x p(1, y) = 0, \tag{3.4c}$$

with the constraint on the range of gap heights, (2.6),

$$\epsilon \leq h(x, y) \leq 1, \qquad \text{for all } (x, y) \text{ in } 0 \leq x, y \leq 1. \tag{3.5}$$

The optimization problem posed in the workshop was find the gap height function $h(x, y)$ to maximize the dimensionless lift,

$$L = \int_0^1 \int_0^1 p \, dy \, dx, \tag{3.6}$$

subject to the constraint of a fixed gap volume (equivalent to the average gap height $\bar{h}$),

$$V = \int_0^1 \int_0^1 h \, dy \, dx = \bar{h}. \tag{3.7}$$

In terms of the dimensionless lift (3.6), the real lift is given by $\mathcal{L} = L_X^2(P_{\text{out}} - P_{\text{in}})L$.

For any specified positive gap volume, the design problem always has a trivial uniform solution $h \equiv \bar{h}$, yielding the pressure field $p(x, y) = 1 - y$. The dimensionless lift for the trivial solution is $L = 1/2$. We will now consider several different approaches to see how we can improve the lift by using different non-trivial gap height profiles $h(x, y)$ motivated by analyses from variational formulations, perturbation methods, and other approaches.

4 Variational formulations of the problem

First, we consider solving the optimization problem directly using the calculus of variations to maximize the lift (3.6) subject to the constraints on h (3.5, 3.7) and the fact that p solves the boundary value problem for Reynolds equation (3.4).

4.1 The one-dimensional variational problem

We begin by reviewing and extending the results found by Robert and Hendriks [10] for the one-dimensional problem, where $h = h(y)$, and $p = p(y)$. In this case, the problem for Reynolds equation reduces to

$$\frac{d}{dy}\left(h^3 \frac{dp}{dy}\right) = 0, \qquad p(0) = 1, \qquad p(1) = 0. \tag{4.1}$$

This problem was formulated as a constrained optimization problem to maximize the lift (3.6), subject to the constraints that the pressure satisfies Reynolds' equation (4.1) and that the volume is fixed (3.7). Hence we wish to find maxima of the integral,

$$I = \int_0^1 p(y) - \lambda(y) \frac{d}{dy}\left(h^3 \frac{dp}{dy}\right) - \mu(h - \bar{h}) \, dy. \tag{4.2}$$

Here μ is a Lagrange multiplier constant for the integral constraint (3.7) and $\lambda(y)$ is a Lagrange multiplier function for the differential constraint (4.1). Another important constraint is the bound on the gap height (3.5), but it is not directly represented in the form of (4.2).

Locally optimal solutions can be obtained via the calculus of variation [8, 13, 16] by setting the first variations of $I(p, h, \lambda, \mu)$ to zero with respect to each of its arguments. Setting $\Delta_\lambda I \equiv \lim_{\delta\lambda \to 0} I(\lambda + \delta\lambda) - I(\lambda) = 0$ yields Reynolds' equation for $p(y)$, (4.1). Similarly, $\Delta_\mu I = 0$ returns the volume constraint, (3.7). The variation with respect to $p(y)$, $\Delta_p I = 0$, yields a boundary value problem for $\lambda(y)$ on $0 \le y \le 1$,

$$\frac{d}{dy}\left(h^3 \frac{d\lambda}{dy}\right) = 1, \qquad \lambda(0) = 0, \qquad \lambda(1) = 0, \tag{4.3}$$

where the boundary conditions result from eliminating boundary terms produced by integration by parts of I. Finally, the first variation of I with respect to $h(y)$ yields

$$\Delta_h I = \int_0^1 \delta h \left[3h^2 \frac{dp}{dy}\frac{d\lambda}{dy} - \mu\right] dy = 0. \tag{4.4}$$

From the fundamental theorem of calculus of variations, the integrand must be zero pointwise everywhere, hence at each point y

$$\text{Either} \qquad (i): \quad \delta h(y) = 0 \qquad \text{or} \qquad (ii): \quad 3h^2 \frac{dp}{dy}\frac{d\lambda}{dy} - \mu = 0. \tag{4.5}$$

Option (i), i.e. that there can be no local variation in h, implies that the value of h is being imposed by the constraint (3.5),

$$(i): \qquad h = \epsilon \qquad \text{or} \qquad h = 1, \tag{4.6}$$

otherwise, for $\epsilon < h < 1$, the local structure of $h(y)$ is determined by

$$3h^2 \frac{dp}{dy}\frac{d\lambda}{dy} - \mu = 0. \tag{4.7}$$

To make this condition more explicit, we note that the closed-form solution of (4.1) for the pressure is

$$p(y) = \frac{\int_y^1 h^{-3}(y')\,dy'}{\int_0^1 h^{-3}(y')\,dy'}, \tag{4.8}$$

and therefore the solution of (4.3) for the the Lagrange multiplier is

$$\lambda(y) = \int_0^y y' h^{-3}(y')\,dy' - \frac{\int_0^1 y' h^{-3}(y')\,dy'}{\int_0^1 h^{-3}(y')\,dy'} \int_0^y h^{-3}(y')\,dy'. \tag{4.9}$$

Substituting these expressions into (4.7) yields

$$-\frac{3}{h^4(y)} \left(\int_0^1 h^{-3}(y')\,dy' \right)^{-1} \left(y - \frac{\int_0^1 y' h^{-3}(y')\,dy'}{\int_0^1 h^{-3}(y')\,dy'} \right) = \mu. \tag{4.10}$$

Since the Lagrange constant μ is currently unspecified, the multiplicative factors can be combined to yield the result that $h(y)$ is given by a fourth root with an integral self-consistency (or compatibility) condition,

$$(ii): \qquad h(y) = C \left| \frac{\int_0^1 y' h^{-3}(y')\,dy'}{\int_0^1 h^{-3}(y')\,dy'} - y \right|^{1/4}, \tag{4.11}$$

where C is some positive constant. This solution is defined on some sub-interval of $0 \le y \le 1$, where $h(y)$ lies in the range $\epsilon \le h \le 1$.

Note that the lift is given by

$$L = \int_0^1 p(y)\,dy = \frac{\int_0^1 y' h^{-3}(y')\,dy'}{\int_0^1 h^{-3}(y')\,dy'}. \tag{4.12}$$

A very interesting consequence of this result is that (4.11) can be written in the form

$$h(y) = C|L - y|^{1/4}. \tag{4.13}$$

It appears that the solutions (4.6) and (4.11) can be "mixed and matched" to construct a piecewise-defined solution almost at will (?)[1] to construct large families of solutions.

We now consider the four basic classes of solutions that can be constructed from (4.6) and (4.11), see Figure 2

[1]It is not clear that there are other mathematical conditions on the solutions imposed by the problem, however, the calculus of variations for non-smooth solutions does have many more subtleties [8].

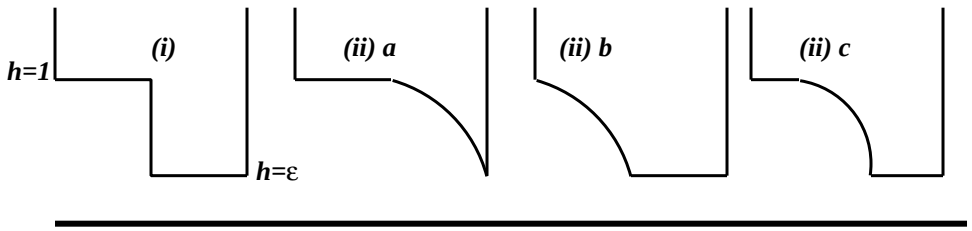

Figure 2: Classes of solutions for $h(y)$, see (4.6, 4.11), suggested by the one-dimensional variational formulation.

4.1.1 Case (i) solutions: the step bearing

The simplest design is a bearing with a single step-discontinuity in the gap height,

$$h(y) = \begin{cases} 1 & 0 \le y \le y_1, \\ \epsilon & y_1 < y \le 1, \end{cases} \tag{4.14}$$

where, the position of jump in h is given in terms of the volume $V = \bar{h}$ by

$$y_1 = \frac{\bar{h} - \epsilon}{1 - \epsilon} \qquad \epsilon \le \bar{h} \le 1, \tag{4.15}$$

and the lift is given by

$$L(\bar{h}, \epsilon) = \tfrac{1}{2} \frac{1 - y_1^2(1 - \epsilon^3)}{1 - y_1(1 - \epsilon^3)} \tag{4.16}$$

Note, that it is possible to construct infinitely many different solutions given by $h = 1$ and $h = \epsilon$ piecewise over different finite sub-intervals of $[0, 1]$, all with the same volume $V = \bar{h}$. All of these solutions have the same value for the integral $\int_0^1 h^{-3}(y')\, dy'$. Consequently, (4.12) shows that the solution that maximizes the first moment of $h^{-3}(y)$ is the one that maximizes the lift. However, this condition does <u>not</u> imply that $h(y)$ must be monotone decreasing, since from (4.12),

$$L = \frac{1}{\int_0^1 h^{-3}(y')\, dy'} \left(\tfrac{1}{2} h^{-3}(1) + \tfrac{3}{2} \int_0^1 y^2 h^{-4}(y) h'(y)\, dy \right); \tag{4.17}$$

If both of the terms in (4.17) are positive, then maximizing L implies minimizing $h(1)$ and requiring $h(y)$ to be an increasing function. However, the second condition implies that $h(1)$ can not be minimized. For decreasing $h(y)$, (4.17) implies a balance between the two oppositely signed terms. Therefore, this leaves open the possibility for other, more complicated classes of solutions that will be addressed in the discussion of the fully two-dimensional problem.

4.1.2 Case (ii)a: non-existence of solutions

A class of monotone decreasing continuous solutions can be constructed by piecing together solutions (4.6) and (4.11). Begin with $h = 1$ for the front portion of the bearing, up to some point where (4.11) takes over, ending at $h(1) = \epsilon$,

$$h(y) = \min \left(1, C \left[1 + (\epsilon/C)^4 - y \right]^{1/4} \right). \tag{4.18}$$

We note that this solution must satisfy the compatibility condition, that the lift given by the integral of the pressure (4.12) is the same as the lift $L = 1 + (\epsilon/C)^4$ in (4.13). However, $1 + (\epsilon/C)^4$ is always greater than one, and the lift given by formula (4.12) applied to the gap height (4.18) is always less than one. Therefore, no such solutions exist.

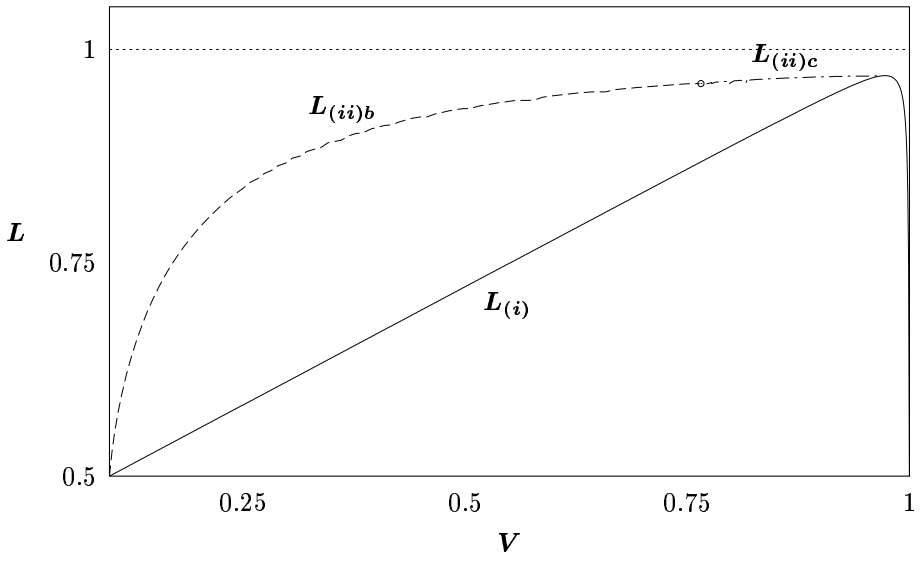

Figure 3: Lift vs Volume for Cases (i), (ii)b, and (ii)c solutions with $\epsilon = 0.1$.

4.1.3 Case (ii)b

Another class of monotone decreasing solutions by can be constructed by piecing together solutions (4.6) and (4.11) in the reverse order. Using (4.11) for the front portion of the bearing, up to some point where $h = \epsilon$ takes over for the finite remaining interval,

$$h(y) = \max\left(C\left[(h_0/C)^4 - y\right]^{1/4}, \epsilon\right). \tag{4.19}$$

This solution is parametrized by the constants C and h_0, where $h(0) = h_0 \leq 1$. This solution can satisfy the compatibility condition, and the resulting lift is $L = (h_0/C)^4$. For a given volume, this solution, if it exists, provides more lift than the corresponding case (i) solution (see Figure 3).

4.1.4 Case (ii)c

The final case we consider is constructed from both sub-cases of (4.6) with solution (4.11) on an interior interval,

$$h(y) = \begin{cases} 1 & 0 \leq y \leq y_1, \\ C(L-y)^{1/4} & y_1 < y \leq y_2, \\ \epsilon & y_2 < y \leq 1. \end{cases} \tag{4.20}$$

For the limiting case, $y_1 = 0$, this solution reduces to case (ii)b, for $y_2 = 1$, it reduces to case (ii)a, and for $y_1 = y_2$ it reduces to case (i). Requiring that (4.20) be continuous determines the constants,

$$L = \frac{y_2 - \epsilon^4 y_1}{1 - \epsilon^4}, \qquad C = L - {y_1}^{-1/4}. \tag{4.21}$$

In order that such solutions exist, they must satisfy the compatibility condition, that is that the lift L given by (4.21) equals the lift given by (4.12). For a given value of ϵ, for the range of volumes where this condition is satisfied, these solutions have a lift greater than or equal to the lift for the type-(i) solutions, see Figure 3. Not surprisingly from the description above about the limiting

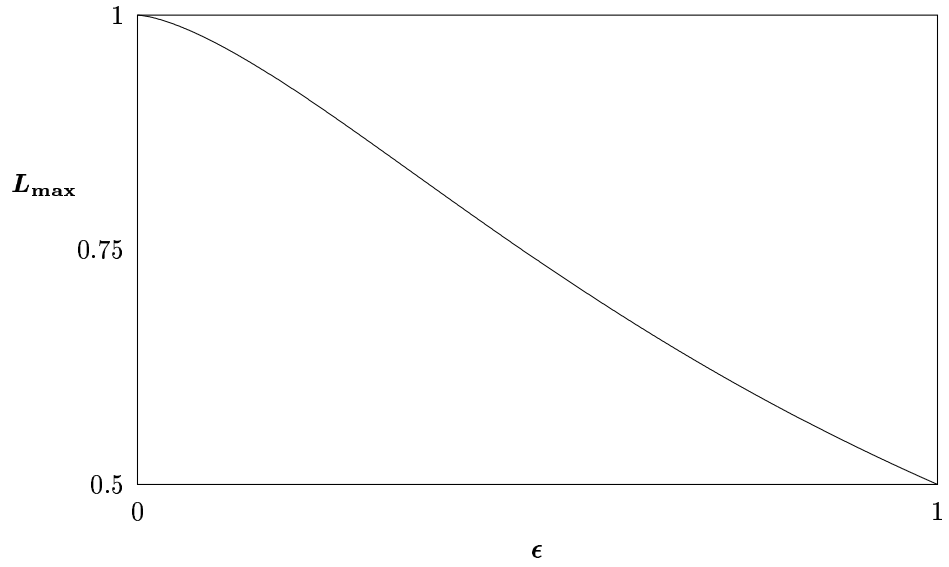

Figure 4: The maximum achievable lift as a function of ϵ, see (4.22).

cases of (4.20), in Figure 3 the lift for this branch of solutions connects the (ii)b solutions to the type-(i) solutions.

4.1.5 Upper bounds for the lift

Figure 3 was calculated for fixed $\epsilon = 0.1$, but the graph of the lift for the different classes of solutions has the same qualitative structure for other values of ϵ. Namely, the maximum achievable lift for fixed ϵ at any volume is attained at the maximum of the lift curve for the type-(i) solution, (4.16). Following some calculations, we find a formula for the maximum possible lift as a function of ϵ (the minimum allowable gap height) (see Figure 4),

$$L_{\max}(\epsilon) = \frac{1}{1+\epsilon^{3/2}}. \tag{4.22}$$

4.2 The two-dimensional variational problem

We can proceed analogously for problems with non-trivial two-dimensional structure, $h = h(x, y)$,

$$I = \int_0^1 \int_0^1 p - \lambda \nabla \cdot (h^3 \nabla p) - \mu(h - \bar{h})\, dx\, dy \tag{4.23}$$

The first variation in λ yields the Reynolds equation for $p(x, y)$, (3.4a). The variation in μ yields the volume constraint (3.7). The setting $\Delta_p I = 0$ yields the boundary value problem for $\lambda(x, y)$,

$$\nabla \cdot (h^3 \nabla \lambda) = 1, \tag{4.24a}$$

with the boundary conditions (derived from Green's first formula)

$$\lambda(x, 0) = 0, \qquad \lambda(x, 1) = 0, \tag{4.24b}$$

$$\partial_x \lambda(0, y) = 0, \qquad \partial_x \lambda(1, y) = 0, \tag{4.24c}$$

Similarly, the first variation with respect h yields

$$\Delta_h I = \int_0^1 \int_0^1 \delta h \left[3h^2 \nabla p \cdot \nabla \lambda - \mu \right] \, dx \, dy = 0 \tag{4.25}$$

from (fundamental theorem of calculus of variations), the integrand must be zero pointwise everywhere, hence

$$\text{Either} \qquad (i): \quad \delta h(x, y) = 0 \qquad \text{or} \qquad (ii): \quad 3h^2 \nabla p \cdot \nabla \lambda - \mu = 0. \tag{4.26}$$

Option (i), that there can be no local variation in h, implies that the value of h is being imposed by the constraint (3.5),

$$(i): \qquad h = \epsilon \qquad \text{or} \qquad h = 1, \tag{4.27}$$

The solution for option (ii) is unclear in two dimensions since closed-form expressions for the pressure, like (4.8), can not be obtained; we will not consider this case further. Instead, in Sections 5 and 6 we will consider the properties of piecewise constant designs with $h(x, y)$ given by (4.27), like the one-dimensional Case (i) solutions considered above.

4.3 Remarks on the variational formulation

Several (theoretically and/or computationally) undesirable features of the design problem as originally posed were noted and considered during the workshop:

1. Numerically obtained solution depend sensitively on the discretization used for the domain and other details of the numerical implementation.
2. The apparent fractal structure of the optimal solution obtained in some computations at IBM [12] (see Figure 8) may be an atypical result tied to the form of the volume constraint.
3. The upper and lower bounds (3.5) on the gap height introduce the possibility for a large multiplicity of non-smooth solutions.
4. The bearing design has discontinuities and sharp edges. This brings into question the validity of of the lubrication approximation and the use of Reynolds' equation to calculate the pressure and the overall lift.

To remove some or all of these undesirable features we make Some suggestions which could remove some of these undesirable features are:

- **The dual problem**

  To investigate features 2 and possibly remove feature 1, we can consider the dual problem: *minimize the volume while keeping the lift constant*.

  In one dimension, a preliminary computation seems to indicate that the solutions of the two problems are identical. But that may not be the case in two dimensions and the numerical behavior of the two problems may be very different.

  Briefly, for comparison with (4.23), the variational formulation of this dual problem is

  $$I_{\text{dual}} = \int_0^1 \int_0^1 h - \lambda \nabla \cdot (h^3 \nabla p) - \mu (p - \bar{p}) \, dx \, dy, \tag{4.28}$$

  where $\bar{p}$, the average pressure, specifies the desired fixed value for the lift.

- **Regularizations**

  The addition to the variational formulation of a term like:

$$-\delta_1 \iint_\Omega \sqrt{1+|\nabla h|^2}\,\mathrm{d}x\,\mathrm{d}y, \tag{4.29}$$

  with δ_1 small, would correspond to a penalization for increasing the surface area of the slider bearing. This term may solve issue 2 and possibly issue 4. It may also erase the fractal character of the design and produce a smooth well-defined solution.

  To address issue 3, we considered the addition of an extra term of the form

$$-\delta_2 \iint_\Omega F(h)\,\mathrm{d}x\,\mathrm{d}y \tag{4.30}$$

  can also be added where $F(h)$ is a quadratic-like function with zeroes $h=\epsilon$ and $h=1$, negative in between those zeroes and positive elsewhere. This term would force the optimum h to lie between ϵ and 1 and would bring some similarities with gradient flows. Potentially this change would determine a smooth solution and eliminate issues of non-uniqueness connected to non-smooth solutions of variational problems [8, 2, 3].

Of course, the validity of these suggestions remains to be established.

5 Analysis of piecewise constant solutions of the 2-d problem

The full problem (3.4–3.7) may be simplified by looking for solutions in which h takes only the two values h_a and h_b, corresponding to (4.27). Then, instead of trying to find a general function of x and y, we only have to select the curve in the x-y plane on which h switches between h_a and h_b.

We label the region where $h=h_b$ as Ω_b and the region where $h=h_a$ as Ω_a. Then Reynolds' equation simplifies to Laplace's equation in each region,

$$\nabla^2 p_b = 0 \quad \text{in} \quad \Omega_b, \tag{5.1a}$$
$$\nabla^2 p_a = 0 \quad \text{in} \quad \Omega_a, \tag{5.1b}$$

where $\Omega_a+\Omega_b=\Omega$ is the unit square, and with the following conditions on the boundary between them (on $\partial\bar{\Omega}$):

$$p_a = p_b, \tag{5.2a}$$
$$h_a^3\frac{\partial p_a}{\partial n} = h_b^3\frac{\partial p_b}{\partial n}, \tag{5.2b}$$

where n indicates the normal direction to the boundary $\partial\Omega$. Now the lift becomes

$$L=\iint_{\Omega_b} p_b\,dx\,dy+\iint_{\Omega_a} p_a\,dx\,dy, \tag{5.3}$$

while the volume constraint yields,

$$h_b\iint_{\Omega_b} dx\,dy+h_a\iint_{\Omega_a} dx\,dy=\bar{h}. \tag{5.4}$$

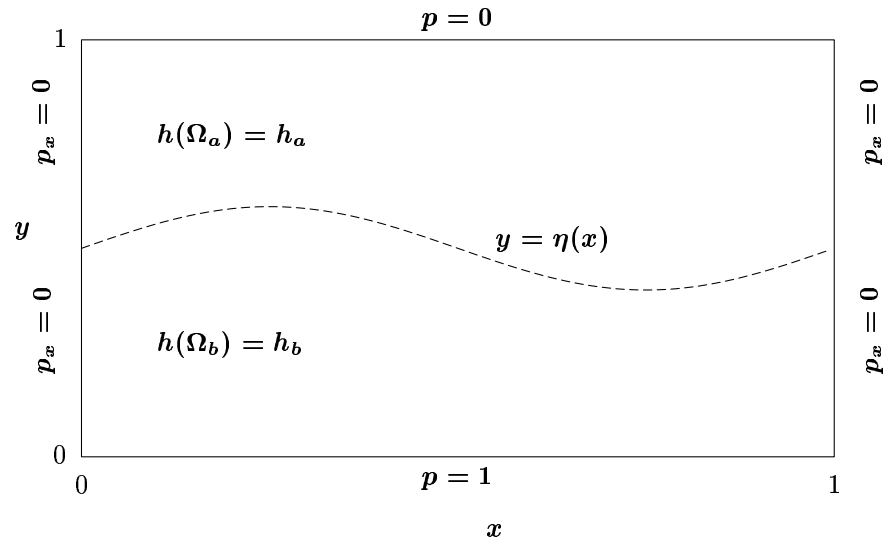

Figure 5: Definition of the geometry in the simplified problem.

We will consider the case where $\partial\Omega$ is a single curve given by $y = \eta(x)$, $0 \le x \le 1$, as illustrated in figure 5, i.e.

$$\Omega_a = \{(x,y)\,|\,\eta(x) \le y \le 1\}, \tag{5.5a}$$
$$\Omega_b = \{(x,y)\,|\,0 \le y < \eta(x)\}. \tag{5.5b}$$

Then the flux condition (5.2b) reads

$$h_b^3\left(\frac{\partial p_b}{\partial y} - \eta'(x)\frac{\partial p_b}{\partial x}\right) = h_a^3\left(\frac{\partial p_a}{\partial y} - \eta'(x)\frac{\partial p_a}{\partial x}\right) \tag{5.6}$$

on $y = \eta(x)$, while the lift to be maximized is

$$L = \int_0^1 \int_0^{\eta(x)} p_b\,dy\,dx + \int_0^1 \int_{\eta(x)}^1 p_a\,dy\,dx, \tag{5.7}$$

and the area constraint reads

$$\int_0^1 \eta(x)\,dx = \frac{\bar{h} - h_a}{h_b - h_a}. \tag{5.8}$$

5.1 Uniform step profiles

Start by considering the simplest possible case, where η is constant, say $\eta = \eta_0$, that is the step bearing (4.14) considered in section 4.1.1. Then the volume constraint specifies

$$\eta_0 = \frac{\bar{h} - h_a}{h_b - h_a}. \tag{5.9}$$

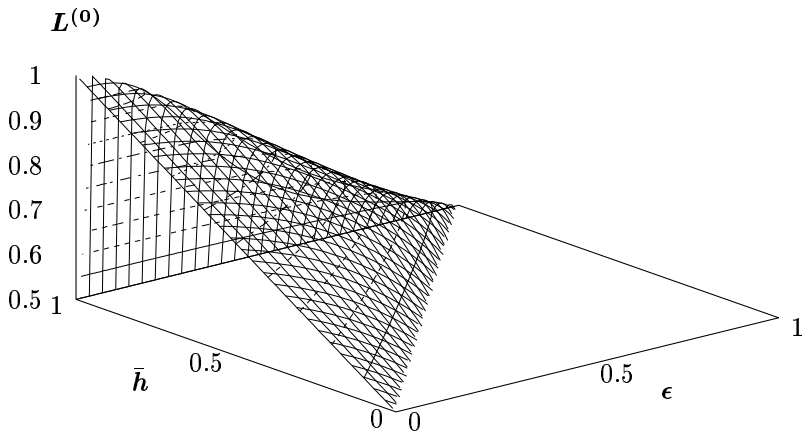

Figure 6: The leading-order lift $L^{(0)}$ plotted as a function of the average gap height $\bar{h}$ with $h_a = \epsilon$ and $h_b = 1$.

It is straightforward to solve for the pressures in this "base" state, which we denote with a superscript zero:

$$p_a^{(0)}(y) = \frac{h_b^3(1-y)}{h_b^3(1-\eta_0)+h_a^3\eta_0}, \qquad \eta_0 < y \le 1, \tag{5.10a}$$

$$p_b^{(0)}(y) = 1 - \frac{h_a^3 y}{h_b^3(1-\eta_0)+h_a^3\eta_0}, \qquad 0 \le y < \eta_0. \tag{5.10b}$$

The lift is given by

$$L^{(0)} = \int_0^{\eta_0} p_b^{(0)}\, dy + \int_{\eta_0}^1 p_a^{(0)}\, dy = \tfrac{1}{2}\,\frac{h_a^3\eta_0^2 + h_b^3(1-\eta_0^2)}{h_a^3\eta_0 + h_b^3(1-\eta_0)}, \tag{5.11}$$

where, from (5.9), η_0 is a known function of h_a and h_b. We plot $L^{(0)}$ versus h_a and h_b in figure 6; without loss of generality, we can impose the normalization condition $h_b = 1$ and $h_a = \epsilon$ and equivalently plot it as a function of the average gap height $\bar{h}$ and the smaller gap height ϵ. The best lift is given by the limit where $\epsilon \to 0$ and this small gap height is imposed over a vanishingly small part of the interval, producing lift $L^{(0)} \to 1$. This is a "sup" for the leading order lift, but it can not actually be obtained.

5.2 Perturbed step profiles

Now suppose the uniform boundary η_0 from §5.1 is perturbed, so that

$$\eta(x) = \eta_0 + \epsilon\cos(kx), \tag{5.12}$$

where $\epsilon \ll 1$ is the amplitude and k is the wavenumber of the perturbation to the flat interface. The question is, does the lift increase or decrease as ϵ is increased from zero? If it decreases, then the uniform solution is locally optimal; it is stable in the sense that an optimization program started with a nearby initial solution would converge to it. If, however, L is an increasing function of ϵ, then the uniform solution is sub-optimal and would not be found by any optimization routine. Furthermore, a clue as to the well-posedness of the optimization problem may be obtained

from the dependence on the wavenumber k. If the lift is enhanced by amplifying arbitrarily large wavenumbers, this suggests that the original problem is ill-posed.

We expand the pressures in the usual way,

$$p_a(x,y) \sim p_a^{(0)}(y) + \epsilon p_a^{(1)}(x,y) + \epsilon^2 p_a^{(2)}(x,y) + \ldots, \qquad \eta_0 < y \le 1, \tag{5.13}$$

$$p_b(x,y) \sim p_b^{(0)}(y) + \epsilon p_b^{(1)}(x,y) + \epsilon^2 p_b^{(2)}(x,y) + \ldots, \qquad 0 \le y < \eta_0 \tag{5.14}$$

where the base solutions are given by (5.10a, 5.10b). The boundary conditions become

$$\begin{aligned} &p_a^{(0)} + \epsilon\left(p_a^{(1)} + \cos(kx)\frac{\partial p_a^{(0)}}{\partial y}\right) + \epsilon^2\left(p_a^{(2)} + \cos(kx)\frac{\partial p_a^{(1)}}{\partial y}\right) + \ldots \\ &= p_b^{(0)} + \epsilon\left(p_b^{(1)} + \cos(kx)\frac{\partial p_b^{(0)}}{\partial y}\right) + \epsilon^2\left(p_b^{(2)} + \cos(kx)\frac{\partial p_b^{(1)}}{\partial y}\right) + \ldots, \end{aligned} \tag{5.15}$$

and

$$\begin{aligned} &h_b^3\left\{\frac{\partial p_b^{(0)}}{\partial y} + \epsilon\frac{\partial p_b^{(1)}}{\partial y} + \epsilon^2\left(\frac{\partial p_b^{(2)}}{\partial y} + \cos(kx)\frac{\partial^2 p_b^{(1)}}{\partial y^2} + k\sin(kx)\frac{\partial p_b^{(1)}}{\partial x}\right) + \ldots\right\} \\ &= h_a^3\left\{\frac{\partial p_a^{(0)}}{\partial y} + \epsilon\frac{\partial p_a^{(1)}}{\partial y} + \epsilon^2\left(\frac{\partial p_a^{(2)}}{\partial y} + \cos(kx)\frac{\partial^2 p_a^{(1)}}{\partial y^2} + k\sin(kx)\frac{\partial p_a^{(1)}}{\partial x}\right) + \ldots\right\}, \end{aligned} \tag{5.16}$$

both evaluated at $y = \eta_0$. The lift is now given by

$$L \sim L^{(0)} + \epsilon L^{(1)} + \epsilon^2 L^{(2)} + \ldots, \tag{5.17}$$

where $L^{(0)}$ is given by (5.11) and

$$L^{(1)} = \int_0^1 \left\{\int_0^{\eta_0} p_b^{(1)}\, dy + \int_{\eta_0}^1 p_a^{(1)}\, dy\right\} dx, \tag{5.18}$$

$$L^{(2)} = \int_0^1 \left\{\int_0^{\eta_0} p_b^{(2)}\, dy + \int_{\eta_0}^1 p_b^{(1)}\, dy + \frac{\cos^2(kx)}{2}\left[\frac{\partial p_a^{(0)}}{\partial y} - \frac{\partial p_b^{(0)}}{\partial y}\right]_{y=\eta_0}\right\} dx. \tag{5.19}$$

Notice that the boundary condition (5.15) has already been used to simplify these expressions. By inspection, the first-order pressures must be of the form

$$p_a^{(1)}(x,y) = c_a \sinh\left[k(1-y)\right]\cos(kx), \qquad \eta_0 < y \le 1 \tag{5.20a}$$

$$p_b^{(1)}(x,y) = c_b \sinh(ky)\cos(kx), \qquad 0 \le y < \eta_0. \tag{5.20b}$$

By plugging these into (5.11, 5.16), we obtain the constants:

$$c_a = \frac{2h_b^3(h_b^2 - h_a^3)\cosh(k\eta_0)}{\left[h_b^3(1-\eta_0) + h_a^3\eta_0\right]\left[(h_a^3 + h_b^3)\sinh(k) + (h_b^3 - h_a^3)\sinh(k - 2\eta_0 k)\right]}, \tag{5.21a}$$

$$c_b = -\frac{2h_a^3(h_b^3 - h_a^3)\cosh(k - k\eta_0)}{\left[h_b^3(1-\eta_0) + h_a^3\eta_0\right]\left[(h_a^3 + h_b^3)\sinh(k) + (h_b^3 - h_a^3)\sinh(k - 2\eta_0 k)\right]}. \tag{5.21b}$$

The periodicity in x clearly implies that the first-order lift is identically zero, $L^{(1)} \equiv 0$, so it is necessary to proceed to $O(\epsilon^2)$.

Again, the general form of the second-order pressures is found by inspection to be

$$p_a^{(2)}(x,y) = d_a(1-y) + e_a \sinh\left[2k(1-y)\right]\cos(2kx), \tag{5.22a}$$
$$p_b^{(2)}(x,y) = d_b y + e_b \sinh(2ky)\cos(2kx), \tag{5.22b}$$

and in terms of the four constants, the lift is given by

$$L^{(2)} = (d_a + d_b)\frac{\eta_0^2}{2} + d_a\left(\frac{1}{2} - \eta_0\right) - \frac{h_b^3 - h_a^3}{4\left[h_b^3(1-\eta_0) + h_a^3\eta_0\right]}. \tag{5.23}$$

Now, by substituting (5.22b) into (5.15, 5.16), we obtain the constants:

$$d_a = -\frac{h_b^3(h_b^3 - h_a^3)^2 k\cosh(k\eta_0)\cosh(k-\eta_0 k)}{[h_b^3(1-\eta_0) + h_a^3\eta_0][(h_a^3 + h_b^3)\sinh(k) + (h_b^3 - h_a^3)\sinh(k - 2\eta_0 k)]}, \tag{5.24a}$$
$$d_b = \frac{h_a^3(h_b^3 - h_a^3)^2 k\cosh(k\eta_0)\cosh(k-\eta_0 k)}{[h_b^3(1-\eta_0) + h_a^3\eta_0][(h_a^3 + h_b^3)\sinh(k) + (h_b^3 - h_a^3)\sinh(k - 2\eta_0 k)]}, \tag{5.24b}$$

while e_a and e_b are horrible expressions[2] which, fortunately, we don't need to determine to obtain the next correction to the lift,

$$\begin{aligned} L^{(2)} = &-\frac{h_b^3 - h_a^3}{4\left[h_b^3(1-\eta_0) + h_a^3\eta_0\right]} \\ &+\frac{(h_b^3 - h_a^3)^2[h_b^3(1-\eta_0)^2 - h_a^3\eta_0^2]k\cosh(\eta_0 k)\cosh(k-\eta_0 k)}{2\left[h_b^3(1-\eta_0) + h_a^3\eta_0\right]^2\left[(h_a^3 + h_b^3)\sinh(k) + (h_b^3 - h_a^3)\sinh(k - 2\eta_0 k)\right]}. \end{aligned} \tag{5.25}$$

The optimality of the uniform base solution is determined by the sign of $L^{(2)}$. When $k = 0$, we have

$$L^{(2)} = -\frac{h_a^3 h_b^3(h_b^3 - h_a^3)}{4\left[h_b^3(1-\eta_0) + h_a^3\eta_0\right]^3} \tag{5.26}$$

which is negative.

5.3 Behavior as $k \to \infty$

If we let $k \to \infty$ in (5.25), we find that

$$L^{(2)} \sim \frac{(h_b^3 - h_a^3)^2[h_b^3(1-\eta_0)^2 - h_a^3\eta_0^2]}{4(h_a^3 + h_b^3)\left[h_b^3(1-\eta_0) + h_a^3\eta_0\right]^2}\,k - \frac{h_b^3 - h_a^3}{4\left[h_b^3(1-\eta_0) + h_a^3\eta_0\right]} + (\text{exponentially small}). \tag{5.27}$$

If the coefficient multiplying k is positive, this indicates that the problem is ill-posed — the lift is maximized by amplifying arbitrarily small wavelengths. So long as w is positive, the only way for the coefficient of k to be negative is for $h_b^3(1-\eta_0)^2 - h_a^3\eta_0^2$ to be negative and then the problem is well-posed. Without loss of generality, we set $h_a = \epsilon$ and $h_b = 1$, then the condition for well-posedness is that $F(\bar{h}, \epsilon) < 0$, where

$$F(\bar{h}, \epsilon) = (1-\eta_0)^2 - \epsilon^3\eta_0^2 \qquad \text{where} \qquad \eta_0(\bar{h}, \epsilon) = \frac{1-\bar{h}}{1-\epsilon}. \tag{5.28}$$

[2] even more so than the above

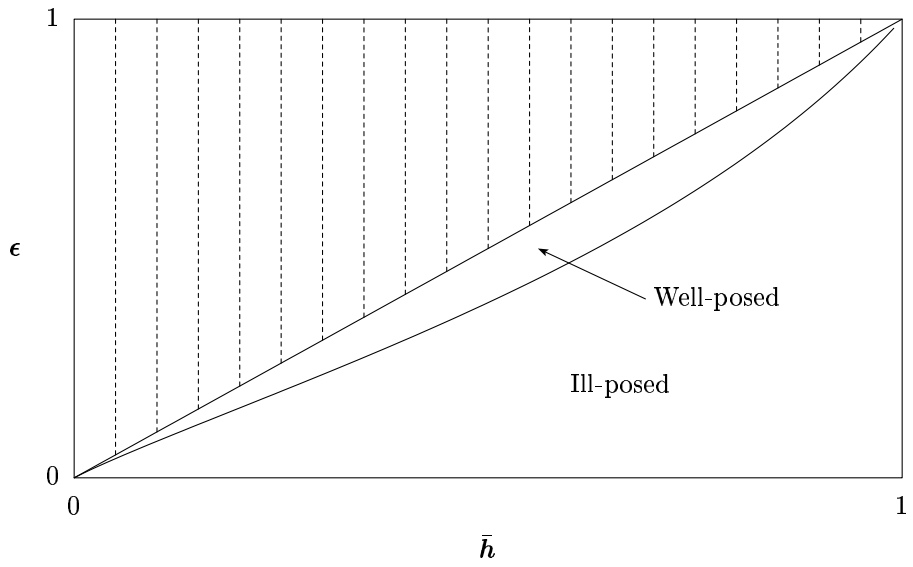

Figure 7: Well-posed and ill-posed regions for step bearing designs in the $(\bar{h}, \epsilon)$ parameter space, with $\epsilon \leq \bar{h}$, separated by the curve $F(\bar{h}, \epsilon) = 0$, (5.28).

Physically reasonable designs require that $0 < \bar{h} < 1$ and $\epsilon < \bar{h}$, and solving $F(\bar{h}, \epsilon) = 0$ yields the boundary curve,

$$\bar{\epsilon}(\bar{h}) = \frac{2\bar{h} - \bar{h}^2 - \bar{h}\sqrt{4\bar{h} - 3\bar{h}^2}}{2(1-\bar{h})^2}. \tag{5.29}$$

From figure 7 we observe that most allowable designs (with $\epsilon \leq \bar{h}$) are ill-posed with respect to small changes in the interface shape $\eta(x)$. For values of $(\bar{h}, \epsilon)$ inside the small "well-posed" region, the optimization problem appears to be well-posed and, indeed, the uniform step solution (4.14) is optimal, at least locally. However, as can be seen from Figure 6, these solutions are definitely not globally optimal since they approach the lower bound for the lift expected from the trivial constant gap height, $L \to 1/2$.

The simple one-dimensional step bearing designs are only well-posed in cases where they have sub-optimal lift. Ill-posedness of the other step-design base states implies that approaching optimal lift more closely will yield non-smooth (possibly fractal?) interface curves $\eta(x)$. One consequence associated with linear ill-posedness of the problem is the possible existence of a large number of solutions. Ill-posedness also means the presence of significant high frequency contributions to (5.12), $k \to \infty$. In terms of numerically implemented solutions, this means that the shortest characteristic length-scale in the solution is solely a consequence of details of the numerical scheme. The conclusion is that some regularization or additional conditions (to reflect other engineering constraints) must be added in order to yield well-defined problems.

6 Air bearing designs based on "gap channels"

Results from some of IBM's computations for the optimization problem suggest that $h(x, y)$ should contain narrow channels where h is large ($h = 1$) surrounding large areas of small gap height ($h = \epsilon$). In fact complex fractal networks of channels were obtained numerically at IBM [12] as potential solutions, see Figure 8. Hence, given the potential complexity of general solutions, we do

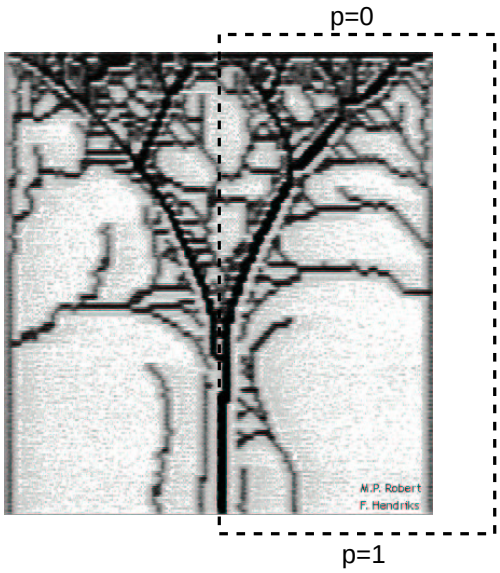

Figure 8: A numerically calculated near-optimal bearing design – courtesy of Robert and Hendriks, IBM Research [12]

not attempt to pursue the full optimization problem [1] (finding $h(x, y)$ that maximizes L), or the reduced inverse problem [5] (finding $h(x, y)$ that yields a given value of L), but instead consider the understanding the forward problem (finding the value of L for a given $h(x, y)$) for a class of bearing designs that approximate the structure of the expected optimal solution. Our first steps in this direction are based on the analysis of a simple gap-height channel with a right-angle corner.

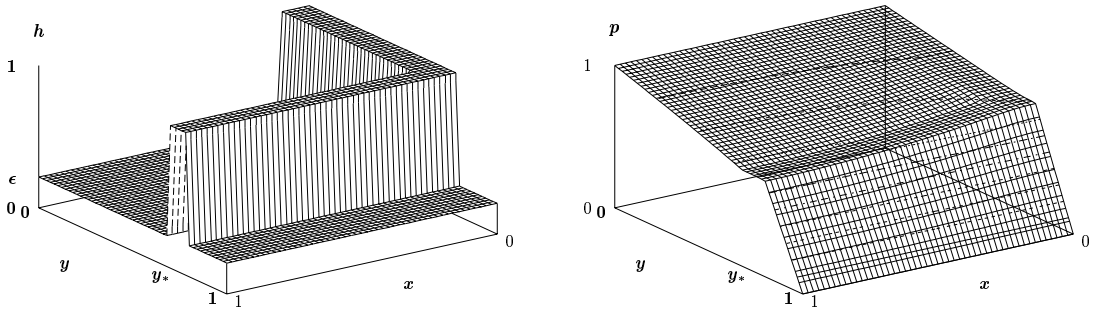

Figure 9: The gap-height $h(x, y)$ and the resulting numerically calculated pressure field $p(x, y)$ for the Model-T design (6.1).

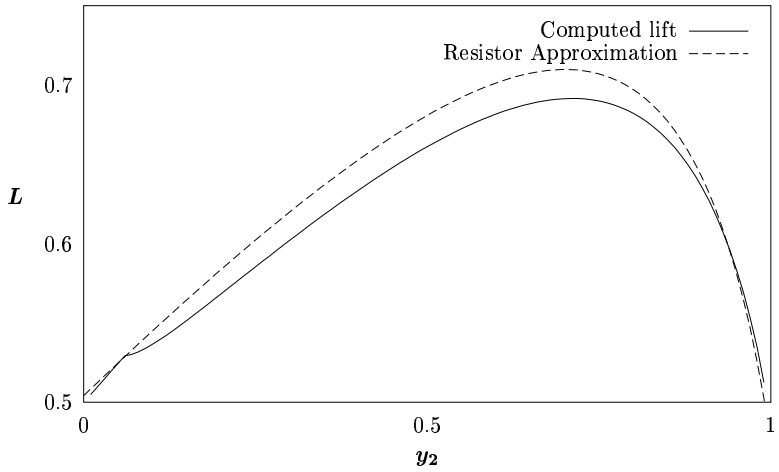

Figure 10: Lift of the model-T channel bearing design (6.1) in terms of the y_2 design parameter.

6.1 The "Model-T" design

We consider the class of bearing designs given by $h(x, y)$,

$$h(x,y) = \begin{cases} 1 & 0 \le x \le w_1 \quad \text{and} \quad 0 \le y \le y_2, \\ 1 & 0 \le x \le 1 \quad \text{and} \quad y_2 - w_2 \le y \le y_2, \\ \epsilon & \text{else}, \end{cases} \tag{6.1}$$

see Figure 9a. For a given value of ϵ, this is a three parameter model (w_1, w_2, y_2) that describes an idealized version of half of a "T-junction" for the primary gap channel shown in Figure 8. The Neumann no-flux boundary conditions at $x = 0$ effectively yield a line of symmetry so that this design does correspond to the basic structure observed in Figure 8.

For lack of analytical techniques to calculate the pressure field and total lift for (6.1), we make use of classical numerical methods to do these calculations. The solution of the elliptic problem (3.4a) for the pressure field can be obtained as the equilibrium solution of the parabolic problem

$$\frac{\partial p}{\partial t} = \nabla \cdot (h^3 \nabla p), \tag{6.2}$$

in the limit that $t \to \infty$. This is sometimes called an "artificial compressibility" technique: given a initial condition that is close to the expected pressure field, the solution will converge arbitrarily closely to the solution for sufficiently large times. In practice the time-scale expected for convergence is inversely related to ϵ, $T = O(\epsilon^{-3})$. The numerical solution of this PDE problem can be efficiently calculated using alternating direction implicit (ADI) methods [7]. For the design (6.1) corresponding to the parameter values shown in Figure 9a, the pressure $p(x, y)$ calculated in this manner is shown in Figure 9b.

A systematic study of the total lift for (6.1) as a function of the design parameter y_2, with $w_1 = w_2 = w = 0.05$ and $\epsilon = (0.01)^{1/3} \approx 0.21$, is shown in Figure 10.

6.2 The resistor network approximation

For designs with piecewise constant gap heights, in each continuous sub-region the pressure is given by the solution of Laplace's equation. Here, we exploit this observation to construct analytical

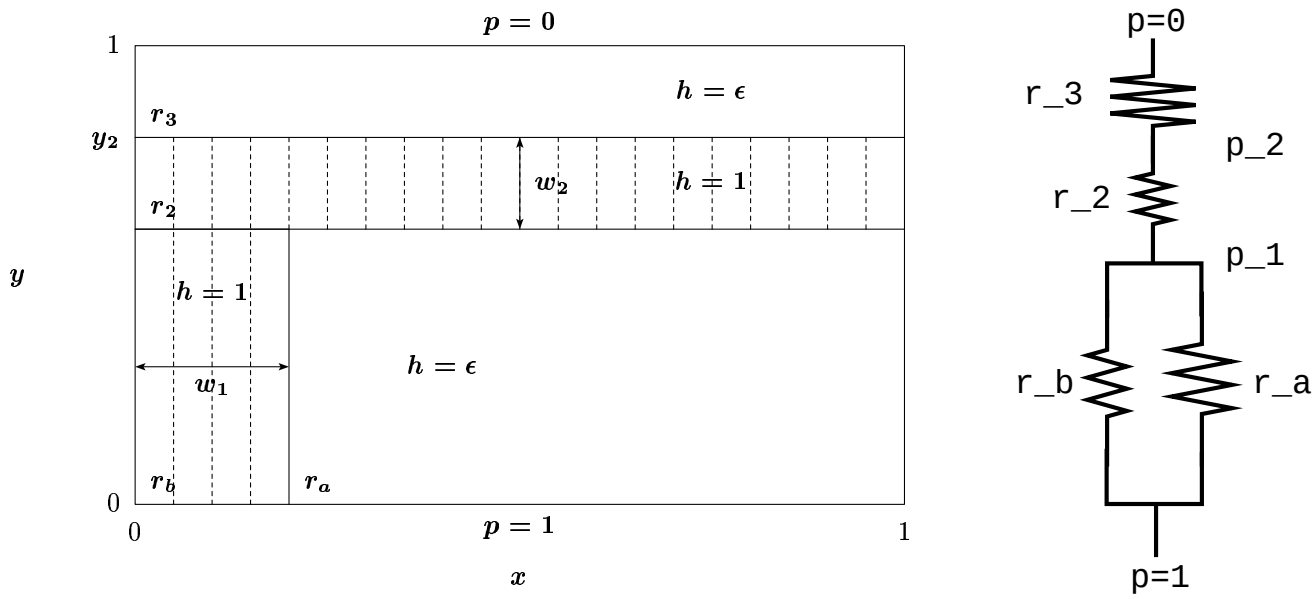

Figure 11: A detailed schematic of the model-T bearing geometry (left) and the corresponding resistor network (right).

approximate solutions for the pressure field. We can construct a pressure solution by appealing to known results for solving Laplace's equation from electrostatics. Specifically, we use Kirchoff's law for the change in potential across a resistor, $\Delta p = I \cdot r$, where I is a measure of the flux. In this context, the pressure p is the potential, and the resistance is inversely proportional to h^3 (i.e. the conductivity or permeability coefficient). From [4], we can define the resistance of a region with uni-directional flux by

$$r = \text{resistance} \equiv \frac{\text{length}}{h^3 \ \cdot \ \text{width}}. \tag{6.3}$$

If we neglect the influence of transverse current flow (flux in the x-direction), then the (6.1) design can be broken down into a network of resistors in the y-direction as shown in Figure 11. The resistances corresponding to the different geometric sections in Figure 11a are given by

$$r_a = \frac{y_2 - w_2}{\epsilon^3(1 - w_1)}, \qquad r_b = \frac{y_2 - w_2}{w_1}, \qquad r_2 = w_2, \qquad r_3 = \frac{1 - y_2}{\epsilon^3}. \tag{6.4}$$

Resistors r_a and r_b are in parallel, therefore they have the same drop in the potential,

$$1 - p_1 = I_a r_a = I_b r_b \tag{6.5}$$

where I_a and I_b refer to the net current (flux) across the respective resistors. Resistors r_2 and r_3 are in series, therefore the drop in the potential is given by

$$p_1 = (I_a + I_b)(r_2 + r_3), \tag{6.6}$$

where p_1 is the value of the pressure at $y_1 = y_2 - w_2$. Using (6.4, 6.5, 6.6), we determine

$$p_1 = \frac{(\epsilon^3 w_2 + 1 - y_2)(1 - w_1 + \epsilon^{-3} w_1)}{y_2 - w_2 + (\epsilon^3 w_2 + 1 - y_2)(1 - w_1 + \epsilon^{-3} w_1)}, \qquad p_2 = \frac{(1 - y_2) p_1}{1 - y_2 + \epsilon^3 w_2} \tag{6.7}$$

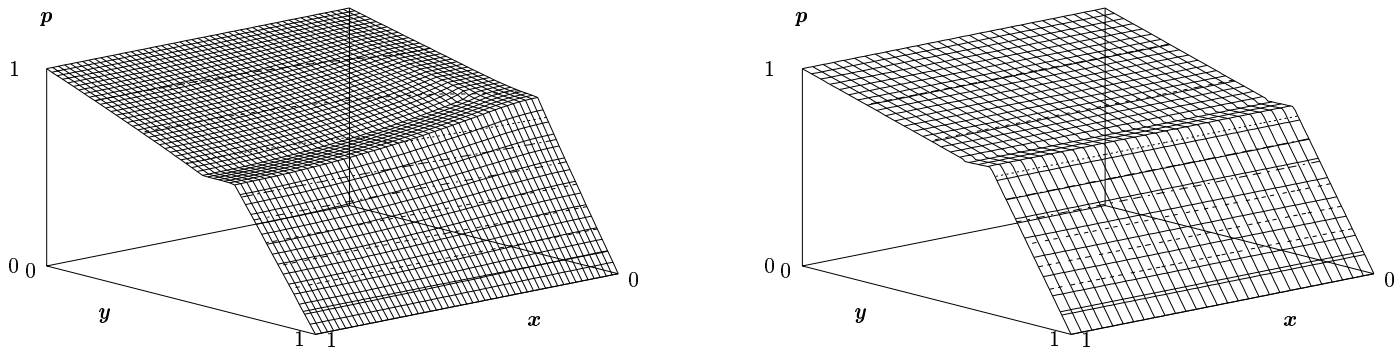

Figure 12: Comparison of the pressure fields for the model-T design shown in Figure 9: (left) results from the ADI numerical computation and (right) the resistor-network approximation (6.8).

The pressure field is then given by

$$p(x,y) = \begin{cases} 1-(1-p_1)y/(y_2-w_2) & 0 \le y \le y_2 - w_2, \\ (p_2-p_1)(y_2-y)/w_2 + p_2 & y_2 - w_2 < y \le y_2, \\ p_2(1-y)/(1-y_2) & y_2 < y \le 1. \end{cases} \tag{6.8}$$

In Figure 12 we show that apart from diffusive "leakage" effects due to air-flow in the x-direction, the solution given by (6.8) gives a good, qualitatively accurate model of the numerically calculated pressure field.

Further, using (6.8), we find that the approximate lift is given by

$$L \approx \tfrac{1}{2}\big(p_1(y_2-2w_2) + p_2(1-y_2+3w_2) + y_2 - w_2\big) \tag{6.9}$$

with the volume of (6.1) given by

$$V = (1-y_2)\epsilon + (1-w_2)(y_2-w_2)\epsilon + w_1(y_2-w_2) + w_2. \tag{6.10}$$

As shown in Figure 10, the resistor-network lift approximation (6.9) is an overestimate of the exact lift (due to the neglect of diffusion in the x-direction), but generally it captures the dependence of the lift on the design parameters quite well. Hence, we conclude that (6.1, 6.7, 6.9, 6.10) could be used as an analytical first estimate of the lift expected for a wide range of designs in the model-T class.

7 Circular air-bearings

We conclude in this section with an examination of the corresponding design problem for circular axisymmetric bearings, i.e. a floating disk above a central air jet. To use lubrication theory, we neglect the region where the air jet impinges on the disk, $0 \le r < R$ (where R is on the order of the radius of the jet). The pressure outlet is taken to be at the outer radius of the disk, $r = 1$.

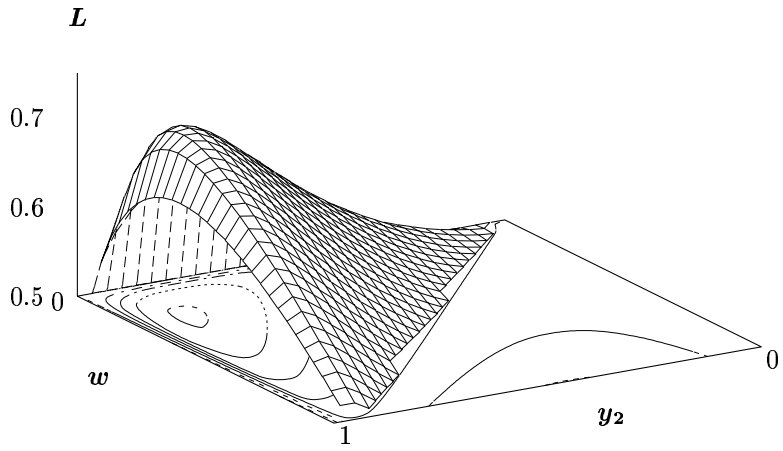

Figure 13: The approximate lift (6.9) given by the resistor model plotted for fixed $\epsilon = 0.15$ as a function of y_2 and $w_1 = w_2 = w$.

7.1 Optimization of an axisymmetric bearing

Similar to Section 3, we seek axisymmetric solutions $p \equiv p(r)$ of (2.2) where $h \equiv h(r)$ on an *annular domain*, $R \le r \le 1$ and $0 \le \theta \le 2\pi$, which maximize the lift

$$L = 2\pi \int_R^1 pr\, dr \tag{7.1}$$

where Ω is an annular domain with Ω_{in} being the inner circle of radius R, and Ω_{out} being the outer circle of radius 1. The constraints on the problem are the boundary conditions

$$p(R) = 1 \qquad p(1) = 0, \tag{7.2}$$

and the constant volume constraint

$$V = 2\pi \int_R^1 hr\, dr. \tag{7.3}$$

If we convert (2.2) into axisymmetric polar coordinates, we obtain

$$\frac{1}{r}\frac{d}{dr}\left(rh^3\frac{dp}{dr}\right) = 0. \tag{7.4}$$

For comparison with section 4, the form of the variational problem in this case is

$$I = \int_R^1 \left[p(r) - \frac{\lambda(r)}{r}\frac{d}{dr}\left(rh^3\frac{dp}{dr}\right) - \mu(h - \bar{h})\right] r\, dr. \tag{7.5}$$

Integrating (7.4), we see that

$$\frac{dp}{dr} = \frac{C}{rh^3} \tag{7.6}$$

where C is a constant of integration. Integrating p over the entire domain and observing that the pressure drop is unity, we find that

$$C = -\left[\int_R^1 r^{-1}h^{-3}\, dr\right]^{-1}. \tag{7.7}$$

Thus, given $h(r)$, the pressure field on the annulus is

$$p(r) = \frac{\int_r^1 s^{-1}h^{-3}\,ds}{\int_R^1 s^{-1}h^{-3}\,ds} \tag{7.8}$$

7.1.1 Optimization for piecewise constant $h(r)$

To optimize $h(r)$ to maximize lift, we shall restrict h to a class of functions with a finite number of parameters, and then choose optimal parameters within this finite dimensional space. Since there is no regularity requirement on h, we shall assume that h is piecewise constant over N evenly intervals from R to 1 with $r_n = R + n\Delta r$ where $\Delta r = (1-R)/N$. If the edges of the intervals are denoted $r_0 = R, r_1, r_2, \ldots, r_N = 1$,

$$h(r) = \begin{cases} h_1 & r_0 \le r < r_1 \\ h_2 & r_1 \le r < r_2 \quad \cdots \\ h_n & r_{n-1} \le r < r_n \quad \cdots \\ h_N & r_{N-1} \le r \le 1 \end{cases} \tag{7.9}$$

the pressure field can be integrated incrementally along these intervals:

$$p(r) = 1 + \int_R^r \frac{C}{sh^3}\,ds$$

$$p(r) = 1 + C\begin{cases} h_1^{-3}\ln\left(\frac{r}{R}\right) & r_0 \le r \le r_1 \\ h_2^{-3}\ln\left(\frac{r}{r_1}\right) + h_1^{-3}\ln\left(\frac{r_1}{R}\right) & r_1 \le r \le r_2 \quad \cdots \\ h_n^{-3}\ln(\frac{r}{r_{n-1}}) + \sum_{m=1}^{n-1} h_m^{-3}\ln(\frac{r_m}{r_{m-1}}) & r_n \le r \le r_{n-1} \end{cases} \tag{7.10}$$

where the normalization constant is

$$C = -\left[\sum_{n=1}^{N} \frac{1}{h_n^3}\ln\left(\frac{r_n}{r_{n-1}}\right)\right]^{-1}. \tag{7.11}$$

In general, if $r_{n-1} \le r \le r_n$,

$$p(r) = 1 + C\left[\sum_{i=1}^{n-1} \frac{1}{h_i^3}\ln\left(\frac{r_i}{r_{i-1}}\right) + \frac{1}{h_n^3}\ln\left(\frac{r}{r_{n-1}}\right)\right]. \tag{7.12}$$

From this, we see that the constant volume constraint (7.3) becomes

$$V = \pi\sum_{n=1}^{N} h_n(r_n^2 - r_{n-1}^2). \tag{7.13}$$

The total lift (7.1) can be integrated directly from (7.12):

$$\begin{aligned} L &= \pi(1-R^2) + \pi C\sum_{n=1}^{N}\frac{1}{h_n^3}\left\{\ln\left(\frac{r_n}{r_{n-1}}\right) - \frac{1}{2}\left(r_n^2 - r_{n-1}^2\right)\right\} \\ &= -\pi R^2 - \frac{\pi C}{2}\sum_{n=1}^{N}\frac{1}{h_n^3}\left(r_n^2 - r_{n-1}^2\right). \end{aligned} \tag{7.14}$$

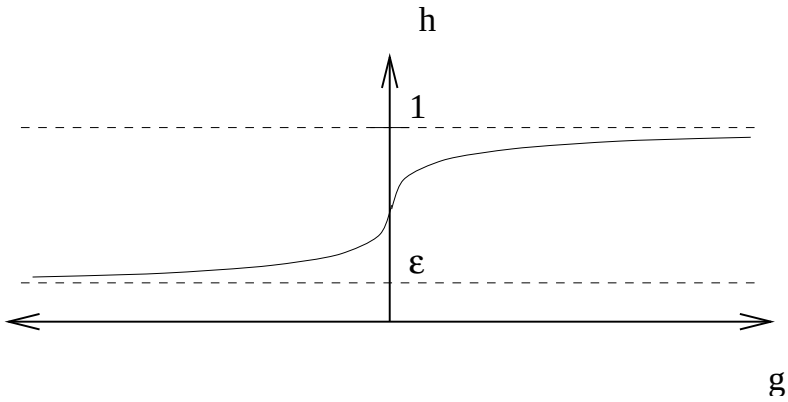

Figure 14: By using a change of variables, $h = h(g)$, the gap height can be automatically restricted to the appropriate range, $\epsilon \leq h \leq 1$.

To solve the reverse problem, we could treat the h_i as tunable parameters as we optimize the function

$$K = L - \lambda(V - V_0)^2 \tag{7.15}$$

where λ is a penalty for the constant volume constraint and V_0 is the desired gap volume. In this case, we could optimize K via a gradient ascent on the h_i parameter space. As $\lambda \to \infty$, we would expect the iterative routine to find a local maximum with gap volume V_0. However, there are further restrictions on h_i (3.5) which are not addressed by this standard formulation. For instance, optimizing K with respect to h_i directly may lead to values of h which are less that ϵ or greater than 1. To address this issue, we re-map h

$$h_i \equiv h(g_i) = \epsilon + \frac{1-\epsilon}{1+e^{-g_i}}, \tag{7.16}$$

so that g_i is the new parameter and h_i is restricted to the proper domain (see Fig. (14)). Furthermore, the mapping is continuous and differentiable allowing us to pursue a modified gradient ascent with the new parameters.

The strategy behind a gradient ascent is to iteratively increase K given some large value of λ. For instance, if we denote all the g_i's as a vector $\mathbf{g}$, a particular vector $\mathbf{g}^{(n)}$ is associated with a certain lift $K(\mathbf{g}^{(n)})$. We seek a new parameter vector $\mathbf{g}^{(n+1)}$ that corresponds to greater lift. Since the gradient K with respect to the parameters is the direction of greatest increase, a simple gradient ascent

$$\mathbf{g}^{(n+1)} = \mathbf{g}^{(n)} + \sigma \frac{\nabla_{\mathbf{g}} K(\mathbf{g}^{(n)})}{\|\nabla_{\mathbf{g}} K(\mathbf{g}^{(n)})\|} \tag{7.17}$$

where σ is a suitably small step size with yield an improved parameter vector, $\mathbf{g}^{(n+1)}$. A few comments about gradient ascents are relevant to this problem [9]:

1. Properly applied, gradients ascents will always find a local maximum or increase without bound. Since the latter is not a possibility for our problem, we are guaranteed to find a local maximum. However, gradient ascent provides no global information.

2. Different initial conditions may lead to different local extrema.

3. Adjusting σ is crucial to the effective use of gradient ascents. If σ is too small, the scheme may require a prohibitively large number of iterations. If σ is too large, the scheme may not smoothly climb the gradient and so will fail to find local maxima.

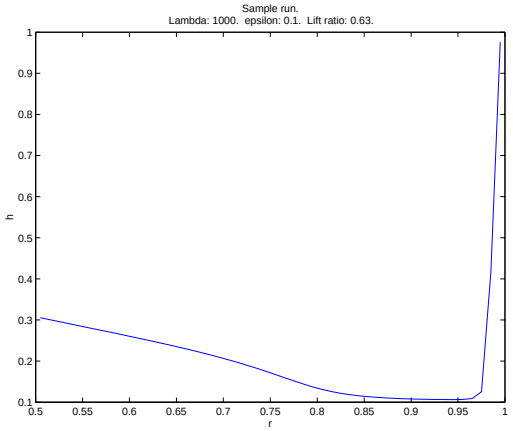

Figure 15: The computed axisymmetric bearing gap height. Here, $R = 1/2$, $\epsilon = 0.1$ and $\lambda = 1000$. The volume is constrained to the value $3\pi/20$.

For this problem, the gradient of K is fairly straightforward.

$$\frac{\partial K}{\partial g_i} = \left[\frac{\partial L}{\partial h_i} - 2\lambda(V - V_0)\frac{\partial V}{\partial h_i}\right]\frac{\partial h_i}{\partial g_i}. \tag{7.18}$$

where

$$\frac{\partial L}{\partial h_i} = \frac{3\pi C}{2h_i^4}\left\{r_i^2 - r_{i-1}^2 + C\ln\left(\frac{r_i}{r_{i-1}}\right)\left[\sum_{n=1}^{N}\frac{1}{h_n^3}\left(r_n^2 - r_{n-1}^2\right)\right]\right\}, \tag{7.19}$$

$$\frac{\partial V}{\partial h_i} = \pi(r_i^2 - r_{i-1}^2), \tag{7.20}$$

$$\frac{\partial h_i}{\partial g_i} = \frac{(1-\epsilon)e^{-g_i}}{(1+e^{-g_i})^2}. \tag{7.21}$$

7.2 Simulated annealing with a low-pass filter

To examine the role of small spatial scale fluctuations in the axisymmetric profile, we turn to simulated annealing. In simulated annealing, we perform a gradient ascent while adding a small amount of stochastic noise:

$$\mathbf{g}^{(n+1)} = \mathbf{g}^{(n)} + \sigma\frac{\nabla_{\mathbf{g}}K(\mathbf{g}^{(n)})}{\|\nabla_{\mathbf{g}}K(\mathbf{g}^{(n)})\|} + C_1 X\exp(-1/T^{(n)}), \tag{7.22}$$

where C_1 is a constant representing the initial amount of thermal noise, X is a random variable, $T^{(n)}$ is a temperature which decreases as n grows. In these applications, all random variables have uniform distributions on $[-1, 1]$, and we found that an effective temperature took the form

$$T^{(n)} = \frac{25\sigma}{n}, \tag{7.23}$$

and $C_1 = 3$ was a sufficient amplitude.

Initial attempts to apply simulating annealing yielded optimized results with large grid-scale deviations. That is, optimal solutions tended to exhibit the highest frequency noise when X was

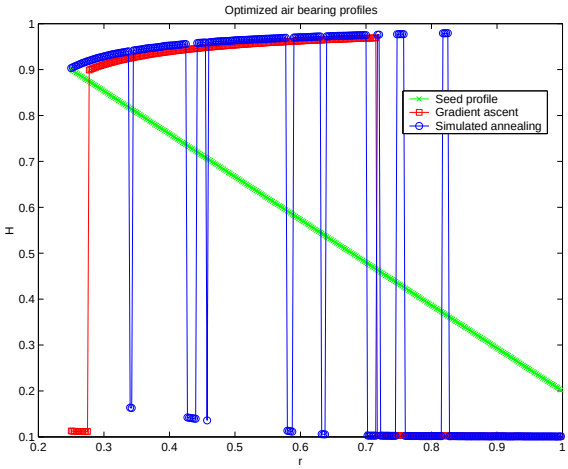

Figure 16: Sample optimized profiles with and without simulated annealing. Both techniques are used to optimize the linear profile shown on the plot. The target volume is $\frac{15}{32}\pi$. The parameter choices are $\epsilon = 0.1$, $R = \frac{1}{4}$ and $\lambda = 1 \times 10^6$. Using gradient ascent and gradient descent with simulated annealing, we optimize an axisymmetric air-bearing. In this example, the lift ratio improves by 13%, rising from 0.578 to 0.658.

a $2N$-dimensional vector of uniform random distributions. This makes sense because the problem is ill-posed, and the optimization algorithm may ascend toward solutions with large gradients. To correct this problem and resolve a reasonable solution for a given mesh, we force X to represent white noise with a high-frequency cut-off that guarantees that any variations will be resolved over at least 5 grid points. That is,

$$X = \frac{5}{N} \sum_{k=0}^{k=N/5} \left[Y_1 \sin\left(\frac{k\pi(r-R)}{1-R}\right) + Y_2 \cos\left(\frac{k\pi(r-R)}{1-R}\right) \right] \tag{7.24}$$

where Y_1 and Y_2 are uniform random variables. In Fig. (16), we can see the advantages of annealing. While it may require several realizations, annealing allows the ascent algorithm to temporarily move away from local basins of attraction toward better optimal solutions. While this does not have many of the characteristics of the full two-dimensionally grooved solutions, it does exhibit deep axisymmetric grooves.

As a final example, we used simulated annealing over a series of step profiles. In Fig. (17), we see that the results are not staggering, but the annealed solutions yielded marginally better lift ratios than the step profiles.

Acknowledgments

Special thanks to Ferdi Hendriks for another interesting and challenging design problem to MPI.

Thanks to Peter Howell[3] for section 5, Lou Rossi for section 7.1 and Domingo Salazar for section 4.3.

[3]And for additional work on the related question of linear ill- or well-posednesss of step slider bearing designs for incompressible flows

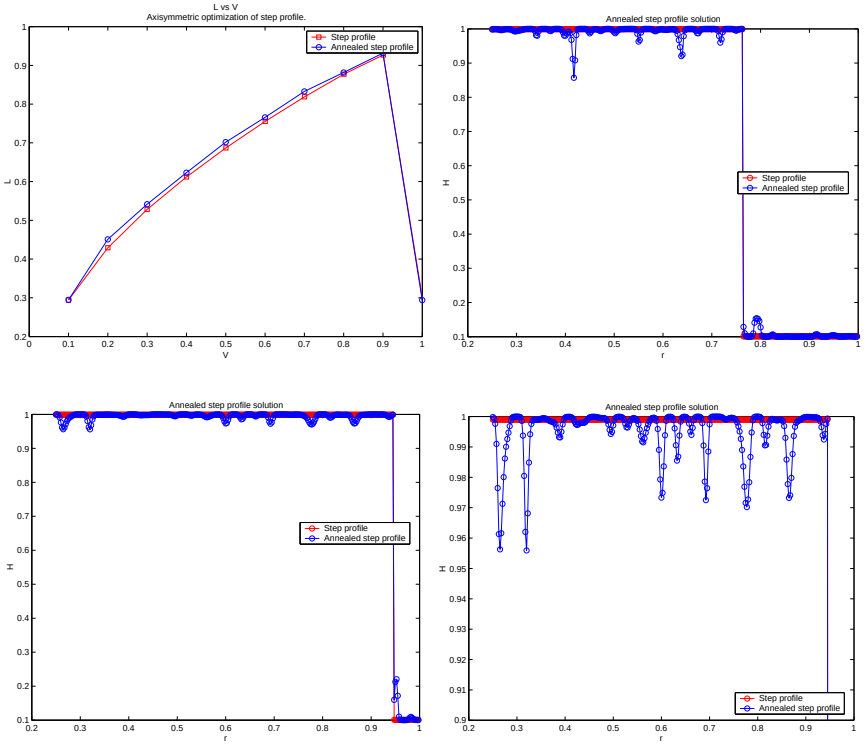

Figure 17: Top-left: Graph of lift (L) versus volume (V) for an axisymmetric step profile, and an annealed step profile. The parameter choices are $\epsilon = 0.1$, $R = \frac{1}{4}$ and $\lambda = 1 \times 10^6$. At top right, one of the annealed profiles is shown. The high-frequency noise plays a major role in improving the lift coefficient. The lower row shows another annealed solution at a higher volume where there is less freedom to manipulate the shape of the bearing. The lower right is a vertically expanded view of the bearing on the left.

A Matlab code for gradient ascents and simulated annealing

This appendix includes some matlab m-files used to generate some of the results in this report. For example, the data generated in Fig. (17) is created with the following commands.

```
r = 0.25:0.01:1;
[Lstep,Vstep,nHstep] = LvV_step(V,r,0.1);
[L,Vact,nHarr] = LvV(V,r,nHstep,1.0e6,0.1,0.3,6.0);
%Now plot L versus V.
plot(Vstep/(15/16*pi),Lstep,'r+-',Vact/(15/16*pi),L,'b+-');
```

The actual profiles are also stored in `nHarr`, so that one can examine them later.

A.1 ascend.m

This subroutine takes an initial profile, and ascend the gradient of the penalty function as described in (7.22). The following table is a list of input/output variables.

r	Mesh
H	Initial $h(r)$ distribution
V0	Desired volume of optimal profile
λ	Penalty constant
ϵ	Minimum height
step	Step size of gradient ascent (σ)
annealScale	Annealing amplitude (C_1)
nH	Optimal profile
pratio	Lift ratio
Lift	Unscaled lift
Vout	Actual volume of optimal profile which may differ slightly from V0

```
function [nH,pratio,Lift,Vout] = ascend(r,H,V0,lambda,epsilon,step,annealScale)

orig = H;
oldK = 0.0;
NumSteps=1;

n = length(H);

if (annealScale ~= 0.0)
    anneal = anneal_fourier(r,annealScale);
else
    anneal = zeros(1,n);
end

[nH,K] = onestep(r,H,V0,lambda,epsilon,step,anneal);
H = nH;

%Set to 1 for diagnostic step.  Set to 0 to iterate.
stop = 0;

while (~stop),
    oldK = K;

    if (annealScale ~= 0.0)
        anneal = anneal_fourier(r,annealScale*exp(-NumSteps/50));
    else
        anneal = zeros(1,n);
    end
    [nH,K] = onestep(r,H,V0,lambda,epsilon,step,anneal);

    if (( (oldK>K) | ((abs(K/oldK-1.0)) < 1.0e-4) ) & (NumSteps > 250) )
        stop = 1;
    end;

    H = nH;
    NumSteps=NumSteps+1;

end;

%Display some information about the optimal state.
n = length(H);

g = -log((1.0-H)./(H-epsilon));

[L,V,dLdg,dVdg] = gradK(r,H,g,epsilon);

Vout = V*2*pi;
Lift = L*2*pi;
pratio = L*2.0/(1.0-r(1)^2);

str = ['Lift: ',num2str(Lift),...
        ' Volume: ',num2str(Vout),...
        ' Pressure ratio: ',num2str(pratio),...
        ' K: ',num2str(L-lambda*(V-V0/2.0/pi)^2)];
% disp(str);
```

```
str = ['Number of steps: ' num2str(NumSteps)];
disp(str);

function [nH,K] = onestep(r,H,V0,lambda,epsilon,step,anneal)

n = length(H);

g = -log((1.0-H)./(H-epsilon));

[L,V,dLdg,dVdg] = gradK(r,H,g,epsilon);

gradKvec = dLdg-2.0*lambda*(V-V0/2/pi)*dVdg;
normgradK = norm(gradKvec);

%Update g's.
g = g + step*(gradKvec)/normgradK + anneal;

nH = epsilon+(1.0-epsilon)./(1+exp(-g));

K = L-lambda*(V-V0/2.0/pi)^2;

function [L,V,dLdg,dVdg] = gradK(r,H,g,epsilon)

n = length(H);

lnr = log(r(2:n+1)./r(1:n));

invH3 = H.^(-3);
invH4 = H.^(-4);

C = -1.0/(lnr*invH3');

dHdg = (1-epsilon)*exp(-g)./(1+exp(-g)).^2;
dVdH = 0.5*(r(2:n+1).^2-r(1:n).^2);

tmp = 2.0*dVdH*invH3';

L = -r(1)^2/2.0 - 0.25*C*tmp;

dLdH = 0.75*C*invH4.*...
    (2*dVdH + C*lnr*tmp);

V = H*dVdH';

dLdg = dLdH.*dHdg;
dVdg = dVdH.*dHdg;

function anneal = anneal_hiband(r,scale)

anneal = scale*2.0*(rand(1,length(r)-1)-0.5);

function anneal = anneal_fourier(r,scale)

n = length(r)-1;
modes=floor(n/5);
anneal = zeros(1,n);
tmp = [1:modes]'*(r(1:n)-r(1))*pi/(r(n)-r(1));
anneal = scale*2.0*((rand(1,modes)-0.5)/modes*sin(tmp)+...
    (rand(1,modes)-0.5)/modes*cos(tmp));
```

A.2 LvV.m

This subroutine applies `ascend` over a range of volumes of initial profiles. Where variable descriptions differ from `ascend`, they are listed below.

Vact	Mesh
H	Initial $h(r)$ distributions
V	Array of desired volumes of optimal profiles
nHarr	Array of optimal profiles
L	Array of lift ratios
Vact	Array of actual volumes of optimal profiles.

```
function [L,Vact,nHarr] = LvV(V,r,H,lambda,epsilon,step,annealScale)

L = V;
Vact = V;
nHarr = zeros(length(V),length(H(1,:)));

for i = 1:length(V)
    str = [num2str(i) ' of ' num2str(length(V))];
    disp(str);
    if (annealScale == 0.0)
        [nH,pratio,Lift,Vout] = ...
            ascend(r,H(i,:),V(i),lambda,epsilon,step,annealScale);
        L(i) = pratio;
        Vact(i) = Vout;
        nHarr(i,:) = nH;
    else
        max = 0.0;
        for j = 1:10
            [nH,pratio,Lift,Vout] = ...
                ascend(r,H(i,:),V(i),lambda,epsilon,step,annealScale);
            if (pratio > max)
                max = pratio;
                L(i) = pratio;
                Vact(i) = Vout;
                nHarr(i,:) = nH;
            end
        end
    end
end
```

A.3 LvV_step.m

This little subroutine generates step profile distributions for comparison with optimized solutions through annealing or whatever technique one finds interesting.

```
function [L,Vact,nHarr] = LvV_step(V,r,epsilon)

L = V;
Vact = V;
nHarr = zeros(length(V),length(r)-1);

%We displace a wee bit because we have remapped the allowable
%using a threshold function that would map 1 and epsilon to
%inf and -inf, respectively.

weebit = 1.0e-3;

for i = 1:length(V)
    r1 = sqrt((V(i)+pi*(r(1)^2-epsilon))./pi./(1-epsilon));
    nHarr(i,:) = 1.0-weebit;
    j = find(r(1:length(r)-1)>r1);
    nHarr(i,j) = epsilon+weebit;

    L(i) = 1-0.5*(2.0*log(r1/r(1))+r(1)^2-r1^2+...
        (r1^2-1-2*log(r1))/epsilon^3)/(1-r(1)^2)/...
        (log(r1/r(1))-log(r1)/epsilon^3);

    L(i) = 1-0.5*((2.0*log(r1/r(1))+r(1)^2-r1^2)./(1-weebit).^3+...
```

```
        (r1^2-1-2*log(r1))./(epsilon+weebit)^3)./(1-r(1)^2)./...
        (log(r1/r(1))./(1-weebit).^3-log(r1)./(epsilon+weebit)^3);

    Vact(i) = pi*((r1.^2-r(1).^2)*(1.0+weebit)+...
        epsilon*(1.0-r1.^2)*(1.0-weebit));
end
```

References

[1] A. Cherkaev. *Variational methods for structural optimization.* Springer-Verlag, New York, 2000.

[2] M. C. Delfour and J.-P. Zolésio. On a geometrical bang-bang principle for some compliance problems. In *Partial differential equation methods in control and shape analysis (Pisa)*, pages 95–109. Dekker, New York, 1997.

[3] J. Goodman, R. V. Kohn, and L. Reyna. Numerical study of a relaxed variational problem from optimal design. *Comput. Methods Appl. Mech. Engrg.*, 57(1):107–127, 1986.

[4] F. Hendriks and T. P. Witelski et al. Design of planar coils of minimum resistance for magnetic recording devices. In *Proceedings of the fifteenth annual workshop on mathematical problems in industry*, pages 1–18. University of Delaware, Dept of Mathematical Sciences, Newark, DE, 1999.

[5] V. Isakov. *Inverse problems for partial differential equations.* Springer-Verlag, New York, 1998.

[6] R. Lipton. Relaxation through homogenization for optimal design problems with gradient constraints. *To appear in Journal of optimization theory and applications*, 2002.

[7] K. W. Morton and D. F. Mayers. *Numerical solution of partial differential equations.* Cambridge University Press, Cambridge, 1994.

[8] E. R. Pinch. *Optimal control and the calculus of variations.* Oxford University Press, 1993.

[9] W. H. Press, S. A. Teukolsky, W. T. Vetterling, and B. P. Flannery. *Numerical Recipes in C, 2nd edition.* Cambridge University Press, Cambridge, 1992.

[10] M. P. Robert and F. Hendriks. Optimization of air bearing grap profile - one dimensional case. *preprint.*

[11] M. P. Robert and F. Hendriks. Gap optimization and homogenization of an externally pressurized air bearing. *Tribology Transactions*, 33(1):41–47, 1990.

[12] M. P. Robert and F. Hendriks. *private communications*, 2001.

[13] L. A. Segel. *Mathematics applied to continuum mechanics.* Macmillan Publishing Co., Inc., New York, 1977.

[14] A. Z. Szeri. *Tribology : friction, lubrication, and wear.* Hemisphere press, Washington, 1980.

[15] N. Wang, C.-L. Ho, and K.-C. Cha. Engineering optimum design of fluid-film lubricated bearings. *Tribology Transactions*, 43(3):377–386, 2000.

[16] R. Weinstock. *Calculus of variations with applications to physics and engineering.* McGraw-Hill Book Company Inc., New York, 1952.